NTA PLASMONX

C. Benedetti, P. Londrillo, S. Rambaldi, G. Turchetti
Sezione INFN Bologna

R. Bonifacio, M. Castellano, A. Clozza, L. Cultrera, G. Di Pirro, A. Drago, M. Esposito, M. Ferrario, D. Filippetto, A. Gallo, G. Gatti, P. Gaudio, A. Ghigo, A. La Monaca, M. Migliorati, D. Nanni, L. Palumbo, M. Richetta, C. Sanelli, F. Tazzioli, A. Tenore, F. Terra, S. Tomassini, C. Vaccarezza, C. Vicario
Laboratori Nazionali di Frascati

A. L. Bacci, F. Broggi, M.M. Cola, A. Flacco, C. Maroli, M. Passoni, V. Petrillo, N. Piovella, R. Pozzoli, M. Romé, A. R. Rossi, L. Serafini
Sezione INFN Milano

D. Batani, A. Galassi, G. Lucchini, R. Jafer, R. Redaelli, R. Benocci, T. Desai
Sezione INFN Milano Bicocca

U. De Angelis, S. De Nicola, R. Fedele, G. Fiore, C. Stornaiolo
Sezione INFN Napoli

S. Betti, C.A. Cecchetti, A. Giulietti, D. Giulietti, A. Gamucci, L.A. Gizzi, P. Koester, L. Labate, T. Levato, A. Macchi, P. Tomassini, M. Vaselli
Sezione INFN and CNR Pisa

1 Summary

The 2008 has been a very fruitful year for the NTA-PLASMONX project. The laser laboratory has been completed and equipped, the laser FLAME assembled and tested at Amplitude Technologies laboratories, the first Laser-Plasma Acceleration experiment (full Italian!) successfully performed in Pisa, new experimental results useful for the project main goals obtained at European laser facilities and at BNL, the design of the e-beam and interaction chamber for the Thomson Scattering based X-ray source completed. Moreover the theoretical and simulation groups have fully supported the experimental activity and anticipated the future scenario of the LPA experiments and X-ray innovative sources that will be carried out in the very next future at LNF. All that will be shortly presented in the following.

2 FLAME

During 2008, construction of the FLAME laser system was carried out at Amplitude Technologies, following requirements and specifications defined during the tender procedure. Several visits of the FLAME team were carried out at Amplitude, including a session for measurements on timing and synchronization, a preliminary acceptance test and a final acceptance test. Final tests included full system energy measurements, survey of the pulse duration optimization procedure, pulse duration measurer nents, including the control-command interface (see Figure 1).

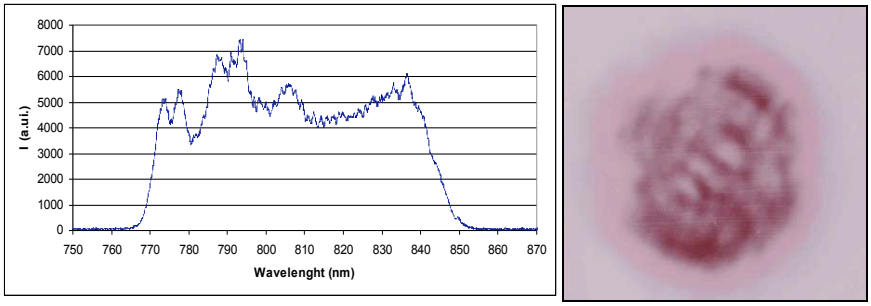

Figure 1: *Left: Spectrum of the laser pulse after amplification showing a bandwidth exceeding 70 nm. Right: Single shot 7 J burn pattern.*

The main parameters of the system measured during the final acceptance test at the factory, during full energy operation at 10 Hz rep. rate are: 5.6 J (energy after compression); 23 fs (pulse duration); 250 TW (peak power), $< 10^{10}$ (ASE contrast); $< 10^{-8}$ (pre-pulse contrast). The average energy (before compression) was measured to be 7.07 J.

3 FLAME laboratory

During 2008 the construction of the FLAME building was completed as shown in the Figure 2 and the design of the entire laboratory layout was carried out including all main subsystems and components: clean room for hosting the laser system, beam transport to the FLAME underground target area and to the SPARC bunker, electricity and ethernet networks, water cooling and air conditioning. Detailed design of the FLAME target area for the planned test experiment on self-injection was also carried out. Procurement for the construction of the beam transport vacuum line and for the set up of the test experiment was started, including the main mirrors, the focusing off-axis parabola and the main experimental diagnostics (see Figure 3).

Figure 2: *FLAME building at LNF completed on 23rd June 2008.*

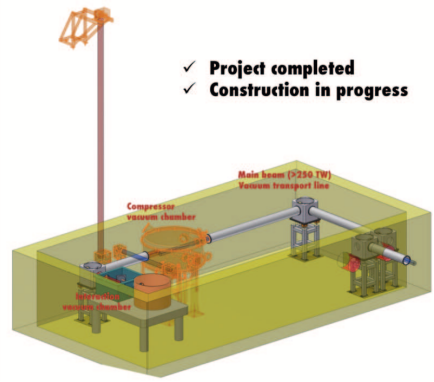

Figure 3: *Design of the layout of the underground target area of the FLAME laboratory, with the main compressor chamber, the vacuum transport line and the target chamber for laser-only experiments.*

4 Laser-Plasma Acceleration Experiment at ILIL-CNR/PISA: First Results from the Plasmon-X Project

4.1 The experimental set up

In the experiment, the main pulse was focused onto a gas-jet target using an F/6 off-axis parabola. The gas-jet target was irradiated at full laser energy varying the gas backing pressure, (i.e. the pressure in the pipe before the fast valve controlling the nozzle) to change the value of the maximum density of the neutral gas. Two gases were used in our experiment, namely He or N_2.

Characterisation of the neutral gas was carried out using optical interferometry. The use of two gases He and N_2, enabled us to explore targets characterised by dfferent physical properties mainly related to the atomic number, and, in particular, to the ionization properties under irradiation of ultrashort, intense laser pulses. The gas-jet nozzle was characterised by a 4 mm long, 1.2 mm wide slit and was mounted on a micrometric motorized support in order to move the interaction point along the three cartesian axes (position scan). During the pulsed operation, the gas flows out of the slit at supersonic speed in order to produce steep interfaces between gas and vacuum. The vacuum in the chamber before the shot is maintained at a pressure below $\approx 10^{-4}$ Torr by a turbo-molecular pump connected to the chamber by a gate-valve.

A full scan of the position of the focal plane along the laser propagation axis and with respect to the top of the nozzle was performed to find the best conditions for acceleration. An important feature consistently observed throughout the experiment is that electron acceleration in our experimental conditions was always found to occur when the focal plane (waist) was located in the proximity of the near edge of the nozzle, typically at ≈ 0.6 mm from the top of the nozzle. A full scan in pressure was also performed, showing that at higher pressure more stable, but less collimated electron bunches are produced. Several diagnostics were used to study the laser-target interaction and the accelerated electrons as shown schematically in Fig. 4. Thomson scattering and Nomarski interferometry were set up perpendicularly to the main laser pulse propagation axis to study and characterize ionisation and basic laser-plasma interaction issues. A second group of

diagnostics including scintillators coupled to photomultipliers, a phosphor screen (LANEX), an electron spectrometer based upon permanent magnets and dose sensitive, radiochromic film stacks (SHEEBA), enabled indirect and direct detection and characterization of the electron bunches accelerated during the laser-gas interaction.

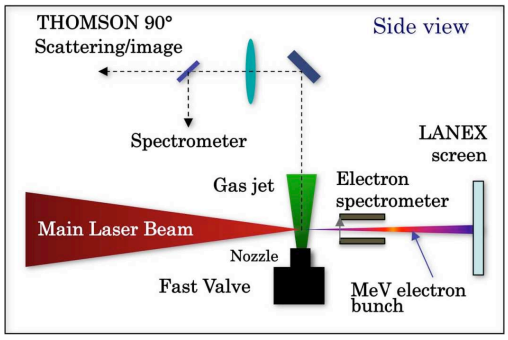

Figure 4: *Design of the layout of the underground target area of the FLAME laboratory, with the main compressor chamber, the vacuum transport line and the target chamber for laser-only experiments.*

4.2 Thomson scattering

Thomson scattering diagnostic was used throughout the experiment to monitor interaction conditions and to identify the basic plasma parameters (see Figure 5). In the classical picture of Thomson scattering, the electrons oscillate in the laser field and, in turn, emit radiation.

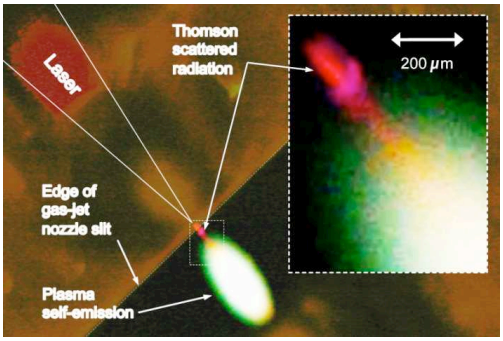

Figure 5: *Typical top-view image of the gas-jet nozzle obtained by the Thomson scattering diagnostic channel showing the main features of the interaction. The waist of the laser beam is placed on the edge of the gas-jet where Thomson scattering radiation is clearly visible (red in colour image). Beyond that point, the laser beam expands and the emission visible in the image is dominated by white light plasma self-emission. The insert in the top-right side of the image shows the magnified region of interaction.*

The properties of this scattered radiation are thus related to the properties of the medium and provide combined information on the laser intensity and electron density. Since in our case, knowledge on the plasma density can be derived independently from the plasma interferometry,

we can use Thomson scattering to derive information on the laser intensity. In our experimental set up an F/10 achromatic doublet was used to produce a 10X magnied image of the interaction region. The image of Fig. 5 shows an overview of the emission produced along the entire laser propagation axis. The waist of the laser beam is placed on the edge of the gas-jet (dashed line in the image) and Thomson scattering radiation is clearly visible as a $\approx 200\,\mu$m long channel-like structure.

A spectral analysis of the accelerated electrons was carried out using a magnetic spectrometer coupled with the LANEX screen (see Figure 6). The spectrometer, based upon permanent NeFeB magnets generating a quasi-uniform magnetic eld ($B_{Max} \approx 0.45$ T), was placed at a distance of 44 mm in front of the LANEX screen. The magnetic field amplitude was mapped in the region of interest using a millimeter-sized Hall magnetic probe. A 2 mm thick Pb foil with a 0.5 mm slit width was placed in front of the magnet, with the slit direction parallel to the magnetic field, in order to limit the transverse momentum of electrons accepted by the electron spectrometer and consequently to increase the resolution of the spectrometer (see Figure 7).

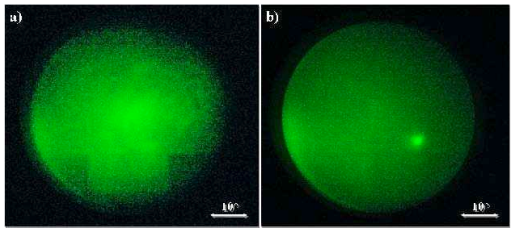

Figure 6: *Typical outputs of LANEX in detection conguration. a) non collimated laser-accelerated electrons in case of N_2 gas at 50 bar. b) collimated laser-accelerated electron bunch in case of He gas at 50 bar.*

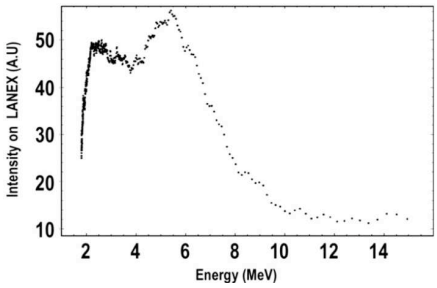

Figure 7: *Electron spectrum obtained with the magnetic spectrometer showing quasi monoenergetic peak between 5 and 6 MeV. The spectrum was obtained from irradiation of a N_2 gas-jet at a backing pressure of 45 bar.*

Numerical modeling based upon particle tracing in the mapped magnetic eld was implemented to describe the performance of the spectrometer in order to obtain the dispersion curve and the intrinsic resolution of both the imaging acquisition system and the LANEX screen. The code also account for errors introduced by beam pointing instability and space-charge effects along

propagation. The results obtained by the magnetic spectrometer were confirmed by independent measurements carried out using an energy spectrometer consisting of sandwiched Radiochromic films (RCF). A sample spectrum obtained with the magnetic spectrometer with N_2 gas-jet is displayed in Fig. 7. According to this spectrum, electrons up to 10 MeV were detected, with an overall spectral distribution characterized by a broad peak with a maximum between 5 and 6 MeV. In some shots, narrower spectral components were found, thought with a poor reproducibility. These results confirm that, in spite of the very low laser intensity compared with most of the experiments available in literature, the electrons accelerated in our experimental conditions are well in the multi-MeV region, with evidence of mono-energetic components emerging clearly from the broad energy spectrum.

4.3 Efficient electron acceleration with 10 TW laser pulses and possible medical applications

In order to improve the characteristics of an electron bunch coming from ultra-intense laser-plasma interaction, an experiment was performed at the SLIC laboratory of CEA Centre in Saclay (France) with a 10 TW Ti:Sa laser system delivering pulses with duration of 65 fs (FWHM) at a wavelength of 800 nm, accounting for a laser strength parameter $a_0 \leq 2$. The experiment, carried out jointly by the ILIL group of CNR, Pisa with the host PHI (Physique a Haute Intensite) group, plus a group from LULI (Ecole Polytechnique, France) and a group from ITU (Institute for Transuranium Elements, Karlsruhe, Germany), allowed the best interaction conditions between the laser pulse and a supersonic gaseous target to be found, and stable and reproducible electron bunches with energy in the range 10-45 MeV to be accelerated (Fig. 8). This task is very important in the context of the comprehension of the mechanisms involved in the laser-plasma interaction and acceleration process (with particular attention to the propagation process) in order to produce high-energy electron bunches. Improvements in the comprehension of such phenomena will be in turn exploited in the frame of the project PLASMONX at ILIL and the Laser Facility that will be soon operating at LNF.

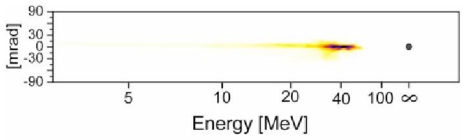

Figure 8: *Representative calibrated image from the magnetic spectrometer. Accelerated electrons show a mono-kinetic component with energy as high as 40 MeV.*

Several advanced diagnostics have been employed to monitor the interaction and the accelerated electron bunches. The photo-activation of nuclear material $^{1}97Au$ driven by the high-energy electrons bremsstrahlung (Fig. 9) in a suitable converter has also been employed to get the number of particles in the bunch with a high degree of accuracy. The total number of electrons with energy greater than 3 MeV was found to be (3.15 ± 0.13) x 10^{10} per laser shot, evinced consistently from all the employed diagnostics. The presented efficient electron source contributes to indicate laser driven electron accelerators, provided them stability and reliability, as a suitable source for medical uses, in particular for Intra-Operative Radiation Therapy (IORT) of tumors. The main properties

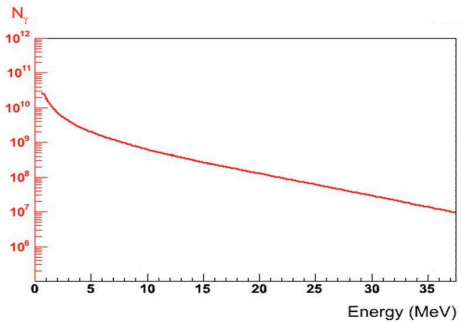

Figure 9: *Spectrum of the bremsstrahlung gamma yield obtained after interaction of the accelerated electrons in a tantalum converter. The number of electrons found after comparison with Monte Carlo tracking code is (3.15 ± 0.13)* $\times 10^{10}$ *per laser shot.*

of commercial RF Hospital accelerated electron bunches for IORT treatment and those of this laser driven accelerator are comparable in terms of bunch charge and electron energy. However, although the dose delivered for each shot is also comparable, the electron bunch duration is about six orders of magnitude lower in the case of the laser-plasma accelerator: few picoseconds versus few microseconds. Thus, the peak current is approximately a million times higher. The radiobiological effects of such difference are still unknown. The new ultrashort laser-plasma electron source thus opens an exciting field of basic bio-medical research.

4.4 Theory and simulations for self-injection experiments

We present some theoretical/numerical studies on electron acceleration (self-injection configuration) with the parameters of the FLAME laser, considering half of the maximum nominal power (P = 150 TW instead of 300 TW), in view of the first LPA experiments which will be carried out during 2009 for the commissioning of the laser system. In order to check the predictions of the scaling laws we have performed several 2D/3D simulations for the 1.2 mm gas-jet. Two-dimensional simulations to study the production of GeV electrons (propagation lengths of $\approx$ 6 mm are required) are underway. All the simulations have been carried out with the fully self-consistent, relativistic, parallelized PIC code ALaDyn. We acknowledge the support of the CINECA computing center for the 3D runs (grant: Simulazioni PIC 3D per l'accelerazione laser-plasma).

- Case 1: We consider $w_0 = 8.9$ μm ($I \approx 1.2 \times 10^{20}$ W/cm^2) and $n_e = 10^{19}$ cm^{-3} (Lgas-jet = 1.2 mm). In Figure 10 (left, center) we show the electron density (XY cut) and the electron energy spectrum. Already inside the plasma (0.7 mm from the beginning of the gas-jet) we observe a monochromatic peak E = (160 ± 5) MeV (FWHM) with a charge of 0.45 nC. Unfortunately we observe also a significant erosion of the laser-pulse front (causing an anticipate dephasing not predicted from the scaling laws) which limits the energy gain for the electrons (160 instead of 400 MeV). This phenomenon has been observed in several 2D simulations when the plasma density is higher than 10^{19} cm^{-3} and the laser is intense. In Figure 10 (right plot) we plot the transverse (x -px) phase space for the monochromatic bunch. The r.m.s. amplitudes of the bunch are $\approx$ 0.8 μm (transverse) and $\approx$ 2.5 μm

(longitudinal), while the normalized emittances are ≈ 5 mm mrad. The (high) value of the emittance is related to the large transverse momentum of the trapped particles and seems to be an unavoidable feature of the bubble regime, however, working at lower laser intensities can give some advantage in this respect.

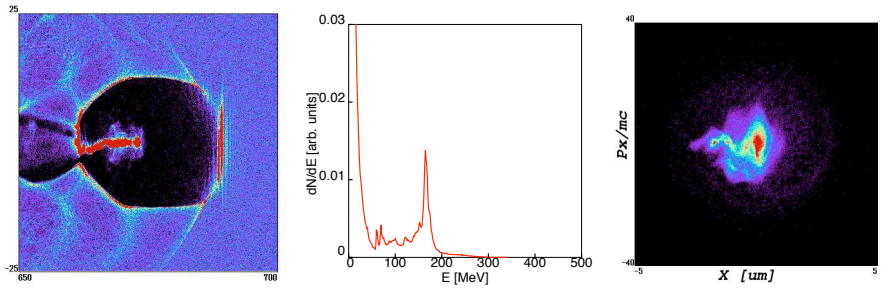

Figure 10: *Case 1:* $w_0 = 8.9\ \mu m$ *(*$I \approx 1.2\ 10^{20}\ W/cm^2$*) and* $n_e = 10^{19}\ cm^{-3}$ *(Lgas-jet = 1.2 mm). (left, center) the electron density (XY cut) and the electron energy spectrum. (right plot) the transverse (x-px) phase space for the monochromatic bunch.*

- Case 2: We consider $w_0 \approx 12\ \mu$m (I $\approx 6 \times 10^{19}$ W/cm^2) and $n_e = 6 \times 10^{18}$ cm^{-3} (Lgas-jet = 1.2 mm). The predicted maximum energy is ≈ 440 MeV and the dephasing length is longer than the gas-jet length so we dont expect a monochromatic beam at the end of the simulation. In Figure 11 we plot the electron spectrum at the exit of the gas-jet and we find a broad peak with an energy of E = (420 ± 40) MeV (FWHM), the corresponding charge is 0.4 nC. Both values are in agreement with theory. The r.m.s. amplitudes of the bunch are ≈ 0.5 μm (transverse) and ≈ 1 μm (longitudinal), the normalized emittances are ≈ 2.5 mm mrad.

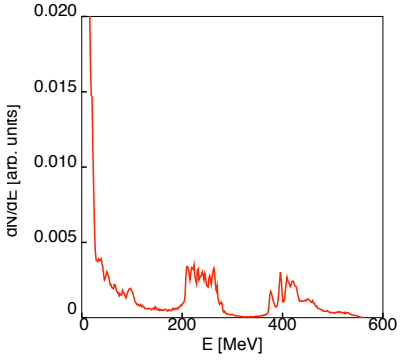

Figure 11: *Case 2:* $w_0 \approx 12\ \mu m\ I \approx 6 \times 10^{19}\ W/cm^2$*)* $n_e = 6 \times 10^{18}\ cm^{-3}$ *(Lgas-jet = 1.2 mm).*

4.5 External Injection: a route for multi GeV high-quality e-beams

4.5.1 Goals and acceleration scheme

The aim for the external-injection studies were the search of an innovative scheme for the generation of multi-GeV beams with promisingly good slice quality and acceptable projected emittances. High-gradient acceleration requires relatively high plasma densities (10^{17}-10^{18}) cm^{-3} that are linked to electron plasma waves in the range (30-100) μm. Since beam-quality requirements are tight, injected beam length is one of the crucial parameters of the scheme and for a 100 μm long wave beam monocromaticity requires injected bunches having lengths not exceeding 2-3 μm rms, a challenging result for current RF-photoinjector technology. Other critical issues are emittance preservation that has been achieved by using an adiabatic injection scheme (i.e. injection in the wake of an adiabatically focusing laser pulse), acceleration length elongation (that should be extended up to 20 Reyleigh lengths via pulse guiding), detailed Langmuir wave phase control that has been obtained via appropriate plasma profile tailoring and jitter of the injection phase. Another issues are nonlinear dynamics of the laser pulse that may undergo self-focusing or phase-modulation and pulse erosion.

4.5.2 Simulation tools

Simulations were performed with the **QFluid** code [P. Tomassini, 2005-2008] that solves in the quasistatic approximation nonlinear equations of fluid response to ponderomotive forces of the laser pulse and beam-loading effects. The **QFluid** code works in a 2D cylindrical space and it has been tested with ALaDyn. The code does not take into account for laser pulse nonlinear dynamics and erosion. While pulse erosion in 10cm should be negligible since the pulse strength a_0 reduces by less the 4% [1D PIC results], detailed self-consistent simulations should be performed for studying pulse nonlinearities.

4.6 Simulation results

A 25 pC, 5 μm and 2.5 μm of rms transverse and longitudinal sizes, energy of 150 MeV and transverse normalized emittance of 1 mm·mrad electron bunch is injected in the second bucket of the Langmuir wave excited by a Ti:Sa pulse delivering 7 J of energy in 30 fs. The laser pulse with initial waist size of 130 μm and minimum size of 32.5 μm is guided by a matched channel profile. The plasma is 9.88 cm long and its density profile has a positive and varying slope with starting and ending densities of 1.5×10^{17} cm^{-3} and 2.5×10^{17} cm^{-3}, respectively. At the final simulation step (see Figure 12) a 2.2GeV electron beam with global energy spread and emittance of 4% rms and 1.5 mm·mrad, respectively, is produced.

Slice analysis with slice thickness of 250 nm reveals the potentialities of the bunch as a driver in X-FEL. While slice emittance is in the range (1.2-1.4) mm.mrad the slice energy spread is in the range (0.02-0.1)% for slices 8-13, with a local current of about 1kA.

5 Ion Laser-Plasma Acceleration

Ion acceleration from solid targets irradiated by high-intensity pulses is a burgeoning area of research, currently attracting a phenomenal amount of experimental and theoretical attention

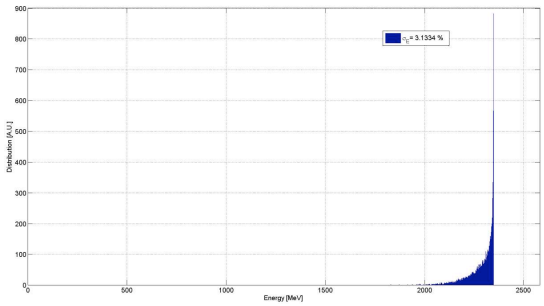

Figure 12: *Energy distribution of the produced e-bunch.*

worldwide. Key to this interest are the ultra-compact spatial scale of the accelerator and the fact that the properties of laser-driven ion beams are, under several respects, markedly different from those of "conventional" accelerator beams. In particular, the spatial quality of laser-driven beams is exceptionally high, and their duration at the source is - down in the ps scale - orders of magnitude shorter than other available sources. In view of such properties laser-driven ion beams have the potential to be employed in a number of innovative applications in the scientific, technological and medical areas, where proton beams with energies greater than 100 MeV are of interest. The FLAME laser could be ideally suited to perform experimental campaigns aimed at improving our basic understanding in this area, towards the achievement of "true" ion beams for applications. In this context, within the PLASMONX project a working group devoted to this subject has been established. A research program has been identified, with the following specific goals:

1. Study and development of dedicated beam diagnostic in order to characterize the quality, the control and the reproducibility of the ion beams, with methods and techniques which are typical of the accelerators physics and technology.

2. Theoretical and experimental investigation of the acceleration mechanisms of ions in the interaction of the ultrashort superintense FLAME laser pulses with solid targets, aimed at the improvement and optimization of the beam properties.

5.1 Theoretical and experimental activity on the TS-source

i) The design of the laser-beam interaction chamber and the devoted e-beam:

A complete design of the interaction chamber, with the focussing solenoid, the bending dipole for the dumping of the beam, the screening of the interaction region and the laser path is presented in Fig. 13. The technical design of the e-beams devoted to the TS based source and the LPA of the external injected electrons has been completed (see Fig. 14).

ii) The development of a procedure of optimization of the X-rays photon flux by means of a genetic algorithm:

In the framework of the maximization of the photon flux of the X radiation produced by the TS source, the genetic code ALGEN has been developed with the aim of optimizing the beam line. The beam line used is similar to that adopted in previous simulations for the

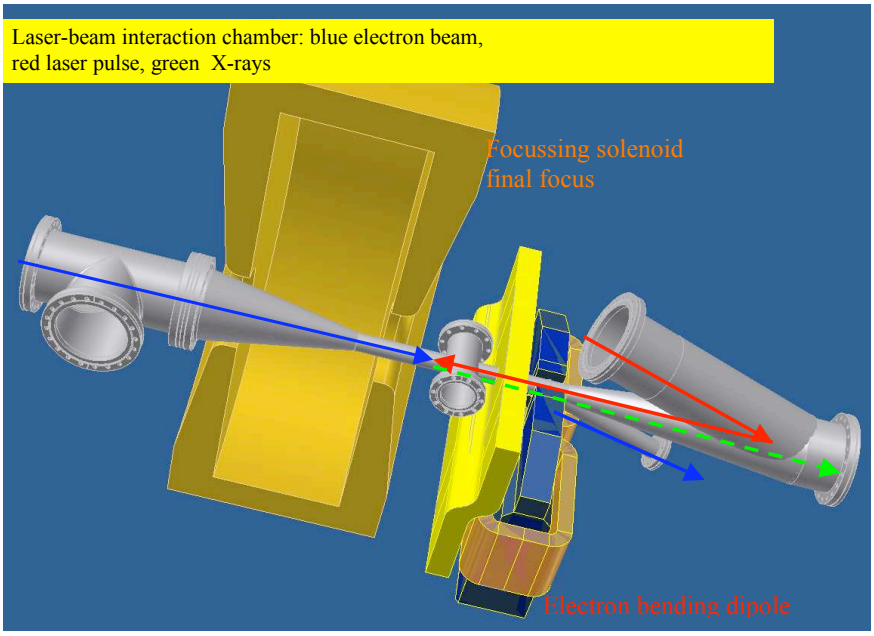

Figure 13: *Interaction chamber for Thomson Scattering based source.*

SPARC/PLASMONX experiment. The bunch has total charge of 1 nC and is extracted from the cathode with a laser pulse of 30 ps. The optimization plays with the following parameters: the gradient of the electric field of the gun $\mathrm{d}E_g/\mathrm{d}z$, the injection phase in the gun Φ_g, the maximum magnetic field of the gun B_g, the gradients of the accelerating structures $\mathrm{d}E_n/\mathrm{d}z$, the injection phase in the structures Φ_n, the maximum magnetic fields B_n, the position of the solenoids zn, and injection phase and position of the forth harmonic cavity Φ_{IVH} and z_{IVH}.

iii) The temporal structure of the X-ray electric field, the field phase and the impact that these characteristics can have on the phase contrast imaging have been considered. For the application to the phase contrast imaging it is very important to determinate the degree of spatial coherence of the radiation. In fact, the electrons of the beam have initial positions and velocities randomly distributed. The inherent randomness of the source will reflect itself on all parameters and measured quantities of the process.

iv) The participation to the measurements of imaging at the TS-source at ATF (BNL, Brookhaven) and the application of these tools to them:

Cooperation with the BNL group working at ATF has been initiated, with the participation of members of the PlasmonX experiment to the measurements made along 2008 on the TS source of Brookhaven. The measurements regard the use of the phase contrast technique for the imaging of wires of various materials and dimensions. A measure of the X rays spot with the traces of the wires has been performed. The X-intensities as given by a phase contrast simulation for a pet wire of dimension of 200 micron have been afterwards evaluated.

v) The investigation of other possible X radiation schemes (All Optical Thomson Source, AOFEL):

Other possible X radiation schemes (All Optical Thomson Source, AOFEL) have been invesigated. In particular we have studied the generation of low emittance high current monoenergetic beams from plasma waves driven by ultra-short laser pulses, in view of achieving beam brightness of interest for FEL applications. The aim is to show the feasibility of generating nC charged beams carrying peak currents much higher than those attainable with photoinjectors, together with comparable emittances and energy spread, compatibly with typical FEL requirements. We have focused on the regime based on a LWFA plasma driving scheme on a gas jet modulated in areas of different densities with sharp density gradients, because it seems more promising in terms of beam emittance. Simulations carried out using VORPAL show, in fact, that in the first regime, using a properly density modulated gas jet, it is possible to generate beams at energies of about 30 MeV with peak currents of 20 kA, slice transverse emittances as low as 0.3 mm.mrad and energy spread around 0.4 %. This beams break the barrier of 1018 A/(mm·mrad)^2 in brightness, a value definitely above the ultimate performances of photo-injectors, therefore opening a new range of opportunities for FEL applications.

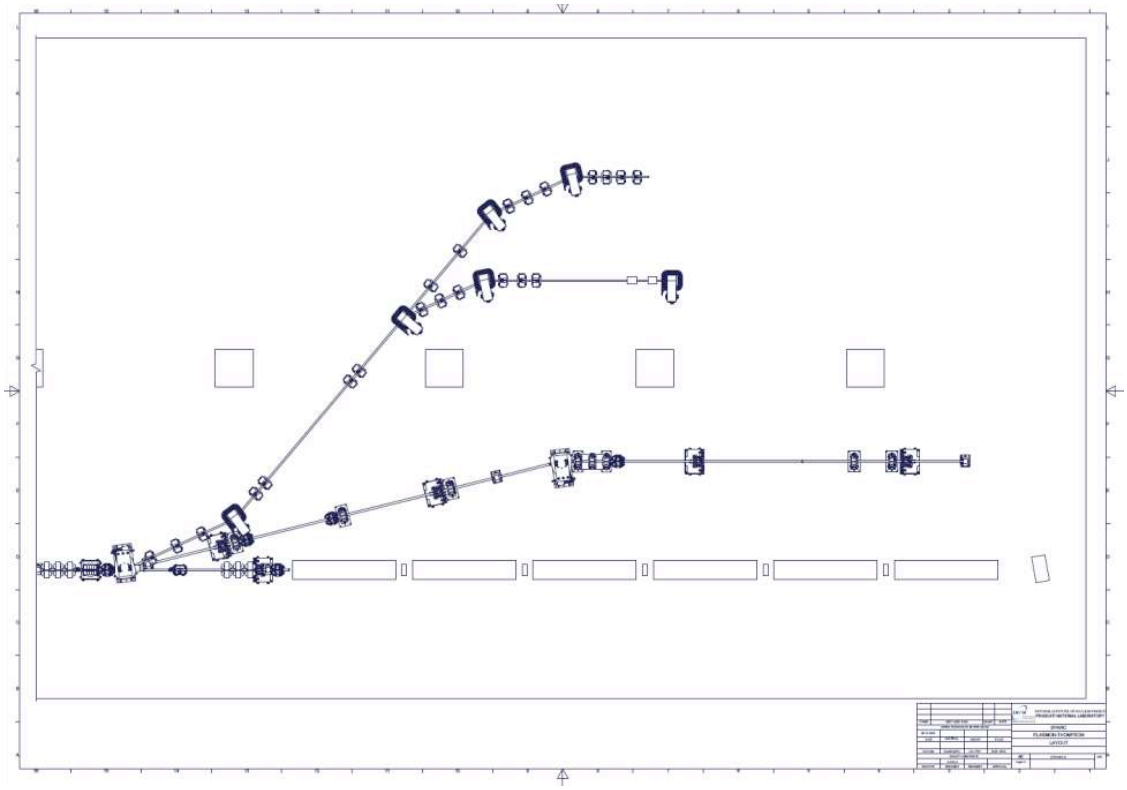

Figure 14: *The technical design of the e-beams devoted to the TS based source and the LPA of the external injected electrons.*

6 References

1. A. Giulietti *et al.*, Phys. Rev. Lett. **101**, 105002 (2008).
2. C. Benedetti, A. Sgattoni, G. Turchetti, and P. Londrillo, IEEE Trans. on Plasma Science, **36**, 1790 (2008).
3. L. A. Gizzi *et al.*, "An integrated approach to ultraintense laser sciences: the plasmon-x project", Europ. Phys. Journal - Special Topics 2009, in press.
4. A. Gamucci *et al.*, IEEE Trans. Plasma Sci. **36**, 1699 (2008).
5. C. Benedetti *et al.*, IEEE Trans. Plasma Sci. **36**, 1790 (2008).
6. C. Benedetti, A. Sgattoni, and P. Tomassini, "ALaDyn: a high accuracy code for the laser-plasma interaction", Proc. of EPAC08, Genova, Italy (2008).
7. C. Benedetti *et al.*, "PIC simulations of the production of high-quality electron beams via laser-plasma interaction", accepted for publication on Nucl. Instr. & Meth. A.
8. A. Bacci, C. Maroli, V. Petrillo, A. Rossi, and L.Serafini, Nucl. Instr. & Meth. in Phys. Res. B **263**, 488 (2007).
9. A. Cedola, I. Bukreeva, S. Lagomarisino, C. Maroli, and V. Petrillo, "Theoretical consideration for X-rays phase contrast mammography by Thomson Source", to be published on Nucl. Instr. & Meth. in Phys. Res. A.
10. P. Tomassini *et al.*, IEEE Trans. on Plasma Science **36**, 1782 (2007).
11. V. Petrillo, L. Serafini, and P. Tomassini, Phys. Rev. Spec. Top. Accel. Beams **11**, 070703 (2008).